Realization of adaptive mesh refinement for phase-field model of thermal fracture within the FEniCS framework

Hirshikesh [a,b,*], Daniel Schneider [b,c], Britta Nestler [b,c,d]

[a] *Department of Mechanical Engineering, Indian Institute of Technology Jodhpur, Rajasthan 342037, India*
[b] *Institute for Applied Materials - Microstructure Modelling and Simulation (IAM-MMS), Karlsruhe Institute of Technology, 76131, Karlsruhe, Germany*
[c] *Institute of Nanotechnology (INT), Karlsruhe Institute of Technology, 76131, Karlsruhe, Germany*
[d] *Institute for Digital Materials Science (IDM), Karlsruhe University of Applied Sciences, Moltkestr. 30, 76133, Karlsruhe, Germany*

Keywords:
Thermal fracture
Phase-field method
Adaptive mesh refinement
FEniCS
Hot cracking

A B S T R A C T

This paper presents an adaptive phase field model for simulating fracture due to coupled interactions (such as thermal quenching and hot cracking in additive manufacturing). The proposed model is implemented in an open-source finite element framework, FEniCS. The model considers spatial variations of the fracture toughness and differential coefficients of thermal shrinkage. Several paradigmatic case studies are addressed to demonstrate the potential of the proposed modeling framework. Specifically, we (a) benchmark our crack predictions for mechanical and thermal boundary condition interactions with the results from alternative numerical methods, (b) accurately reproduce experimentally observed complex crack trajectories due to thermal quenching and hot cracking in additive manufacturing, and (c) demonstrate the ease of extending of the proposed framework to thermal cracking problems in three dimensions. The current implementation provides the basic for an efficient framework for fracture problems due to multi-physical interactions for practical engineers with less programming expertise.

1. Introduction

Owing to its applicability in various engineering fields such as thermal quenching [1], additive manufacturing (AM) [2], and casting [3], fracture prediction due to transient thermal load has attracted a lot of interest from both the industry and academic researchers to reduce the production costs and prevent in-service failures. The AM process introduces several defects including porosity, inclusion, residual stress, and hot cracking. Among these, hot cracking stands out as one of the most prevalent defects, impeding the widespread applicability of the AM. The hot cracking is the result of the interplay between the crack driving forces due to the thermal stresses and the material's resistance to fracture. Several experimental investigations are reported to explain hot cracking mechanisms by performing microstructural analysis and hot cracking susceptibility [4–6]. In thermal failure, the material's interior is penetrated by several intricate cracks, making it challenging to predict with conventional finite element simulations. However, the extended finite element method (XFEM), which is used to simulate crack growth problems with multi-physical interactions such as thermal fracture for orthotropic materials [7], piezoelectric materials [8], and thermal quenching [1,9], addresses some of the shortcomings of the conventional FEM (e.g., the requiring of a particular type of element at the crack tip, re-meshing as the crack propagates). Though XFEM can handle complex cracking events due to multi-physical interactions, it necessitates using an enrichment function for the crack tip, split elements, ad-hoc criteria for the crack nucleation, propagation

* Corresponding author at: Department of Mechanical Engineering, Indian Institute of Technology Jodhpur, Rajasthan 342037, India.
E-mail address: hsk111989@gmail.com (Hirshikesh).

direction, branching, and merging. Different standards result in various crack paths [10]. The phase-field method (PFM), regularized with the help of a scalar field variable, provides an alternative approach to simulate aforementioned cracking events elegantly [11]. Since its inception, the PFM has been applied to various problems such as the dynamics of brittle fracture [12–14], fracture in biological tissue [15], failure of composite [16,17]. The PFM is also extended to encompass fatigue crack growth [18]. Furthermore, Li et al. [19] conducted an extensive review of the recent work on PFM models used to understand fatigue crack growth. Miehe et al. [20–23] postulated the PFM towards multiphysics problem in which stress-based constitutive driving force is incorporated for multi-physical interactions. Recently, Ruan et al. [24] applied the PFM model to simulate hot cracking during the additive manufacturing (AM) process.

However, the conventional PFM is computationally expensive because it requires (a) solving an additional partial differential equation, i.e., evolution equation, (b) resolving the computational domain with a required extremely refined mesh to accurately approximate the length scale parameter, ℓ_c in the fracture process zone. The computational efficiency can be improved by either local refinement of the mesh [25] or by adaptive time stepping [26–28]. The local mesh refinement within the PFM framework has received considerable attention [16,29–32]. Nevertheless, adaptive mesh refinement may require efficient solvers and preconditioners to expedite the solution process, as the number of elements could significantly increase [33,34]. To this end, several efficient solvers for the PFM have been proposed, e.g., the work by Berger-Vergiat and Waisman [35] and Svolos et al. [36] elaborating an overlapping domain decomposition approach for the parallel solution of dynamic fracture problems. Furthermore, matrix-free geometric multigrid solvers in [37], and an accelerated staggered scheme [38] can be found in recent literature. Hirshikesh et al. [39] implemented PFM without adaptive mesh refinement scheme in an open source finite element package FEniCS [40]. Tangella et al. [41] extended phase-field FEniCS implementation for thermal fracture. On the other hand, Freddi and Mingazzi [42,43] implemented the adaptive phase-field in FEniCS to understand fracture due to mechanical forces or applied displacement. The elements that need to be refined and identified are based on energy criteria and distance, which are within a distance based on $\beta_3\ell$, where β_3 is a constant and ℓ is the characteristic length scale. The distance between the centroid of finite elements is evaluated using SciPy cKDTree. It is worth noting that the implementation is limited to addressing the two-dimensional fracture problem. To this end, the main aim of the manuscript is to implement the adaptive phase-field model in open-source platforms for fracture due to multi-physical interactions with a particular focus on addressing three-dimensional problems. Therefore, the objectives of this manuscript are (a) to develop adaptive mesh refinement strategies for solving thermal cracking problems, (b) to implement the framework in the open-source finite element software, FEniCS, and (c) to propose an approach for solving hot cracking in AM to reduce the computational costs associated with conventional PFM.

We believe that establishing a process that can use an efficient open-source platform with adaptivity can improve the efficiency of the solution process of fracture problems, resulting in many potential benefits for practicing engineers. In this work, we use FEniCS (an open-source finite element package) to implement adaptive PFM based on strain energy density and phase-field variables. FEniCS is a limited element-based automated solutions framework for the partial differential equations (PDEs) [40]. In FEniCS, the user has to specify the variational form along with the relevant geometry, boundary conditions, and mesh information through the Python or C++ interface. FEniCS takes care of the element stiffness matrix calculations and assembles them to obtain the global stiffness matrix. Another significant advantage of FEniCS is its capability to extend from two-dimensional to three-dimensional analysis seamlessly. This feature is valuable when solving three-dimensional fracture problems requiring adaptive mesh refinement. By leveraging this capability, researchers can efficiently tackle complex three-dimensional fracture scenarios while benefiting from the adaptability and ease of use provided by the FEniCS framework.

The rest of the paper is organized as follows: Section 2 presents a brief overview of the phase field method for fracture. The adaptive refinement strategies for thermal problems in FEniCS are presented in Section 3. Section 4 presents numerical results for various test cases in two and three dimensions and a concluding remark with future outlook is shown in the last Section 5.

2. Model formulation

Consider a linear elastic solid body $\Omega \subset \mathbb{R}^d$ with an external boundary $\Gamma \subset \mathbb{R}^{d-1}$ as shown in Fig. 1, where d is the dimension of the problem. Let Γ_u, Γ_t, Γ_T, and Γ_q be the displacement, traction, temperature, and heat flux boundaries, respectively. The boundary Γ admit the following decomposition with the outward normal $\boldsymbol{n}$: $\Gamma_t \cup \Gamma_u = \Gamma$, $\Gamma_t \cap \Gamma_u = \emptyset$, $\Gamma_q \cup \Gamma_T = \Gamma$, and $\Gamma_q \cap \Gamma_T = \emptyset$. The phase-field method (PFM) framework utilizes a scalar continuous field variable called the phase-field variable $\phi(\boldsymbol{x}, t) \in [0, 1]$ to approximate the sharp crack topology, as depicted in Fig. 1. In this representation, $\phi = 0$ corresponds to the intact material, while $\phi = 1$ represents the fully damaged state of the material. The coupled governing equations that govern different fracture events due to thermo-mechanical interactions are expressed as

$$\nabla \cdot \boldsymbol{\sigma} = \boldsymbol{0} \quad \text{in} \quad \Omega, \tag{1}$$

$$\rho c_p \dot{T} + \nabla \cdot \boldsymbol{J} = 0 \quad \text{in} \quad \Omega, \tag{2}$$

$$g'(\phi)H + \frac{\mathcal{G}_c}{c_\alpha}\left(\frac{1}{\ell_0}\alpha'(\phi) - 2\ell_0\nabla^2\phi\right) = 0 \quad \text{in} \quad \Omega, \tag{3}$$

where for the displacement field sub-problem the following notation is applied: $\boldsymbol{\sigma} = g(\phi)\mathbb{D} : (\boldsymbol{\varepsilon} - \boldsymbol{\varepsilon}^{\text{th}})$: Cauchy stress tensor, $\boldsymbol{\varepsilon} = \text{sym}\nabla\boldsymbol{u}$: small strain tensor, $\mathbb{D}$: elastic stiffness matrix, $g(\phi) = ((1-\phi)^2 + k_{\text{res}})$: degradation function with k_{res} being a small number introduced for numerical stability, $\boldsymbol{\varepsilon}^{\text{th}} = \alpha(T - T_0)$: thermal strain, α: coefficient of thermal expansion. In the thermal field sub-problem: the flux is denoted as $\boldsymbol{J}$, and determined as $\boldsymbol{J} = -g(\phi)K\nabla T$. Here the flux is degraded to ensure discontinuity of the thermal field across the

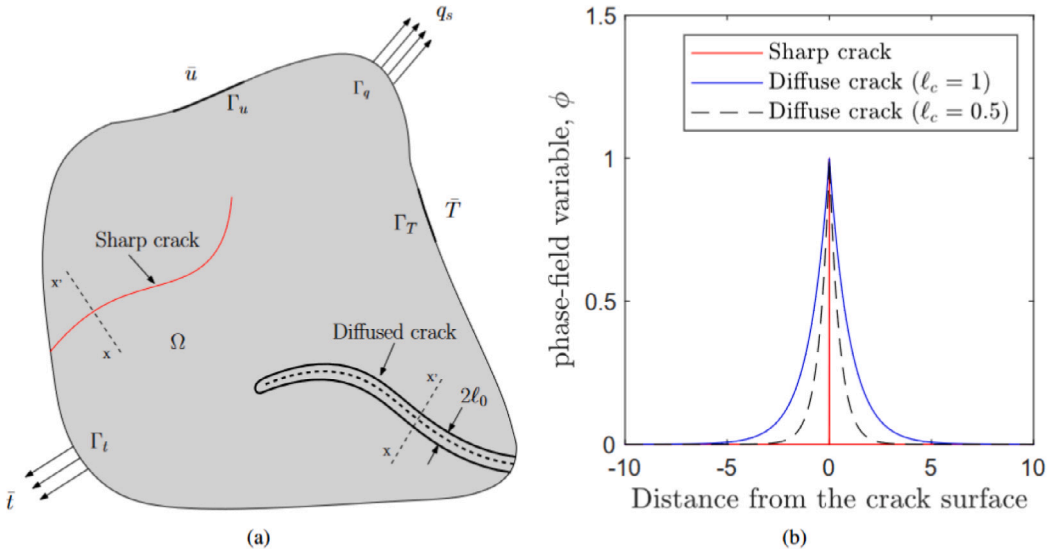

Fig. 1. (a) Schematic representation of the cracked thermo-elastic domain with the sharp and diffused representation of the crack, and (b) the approximation of the sharp and diffuse crack along xx' line. Here $\phi \in [0, 1]$: phase-field variable, and ℓ_0 denoted the length scale parameter.

crack surface. The additional parameters in this equation denote K: thermal conductivity, ρ: density, and c_p: specific heat at constant pressure. In the phase-field evaluation equation, the following terms involve $\mathcal{G}_c$: critical energy release rate, H: crack driving force, and for AT2 model $\alpha'(\phi) = \phi^2$ and $c_\alpha = 2$. The crack driving force, as currently defined, does not differentiate between the tensile and compressive components. However, this can be achieved by implementing a tension–compression splitting approach for the crack driving force [20,44]. In this work, the crack driving force is decomposed as follows:

$$H^{\pm} := \max_{\tau \in [0,t]} \psi_0^{\mathrm{el}\pm}(\boldsymbol{\varepsilon}^e), \quad \text{and} \quad \psi_0^{\mathrm{el}\pm} = \frac{1}{2}\lambda \langle \mathrm{tr}(\boldsymbol{\varepsilon}^e)\rangle_{\pm}^2 + \mu \mathrm{tr}((\boldsymbol{\varepsilon}^e)_{\pm}^2), \quad \text{and} \quad \boldsymbol{\varepsilon}^e = \boldsymbol{\varepsilon} - \boldsymbol{\varepsilon}^{\mathrm{th}}, \tag{4}$$

where λ and μ are the Lamé constants.

By exclusively taking into account of tensile component, the evolution equation can be re-written as

$$g'(\phi)H^{+} + \frac{\mathcal{G}_c}{c_\alpha}\left(\frac{1}{\ell_0}\alpha'(\phi) - 2\ell_0\nabla^2\phi\right) = 0 \quad \text{in} \quad \Omega, \tag{5}$$

The coupled governing equations Eqs. (3) and (5) with the following boundary conditions are solved using the staggered approach

$$\boldsymbol{u} = \bar{\boldsymbol{u}} \quad \text{on} \quad \Gamma_u, \tag{6a}$$

$$\boldsymbol{\sigma} \cdot \boldsymbol{n} = \bar{\boldsymbol{t}} \quad \text{on} \quad \Gamma_t, \tag{6b}$$

$$\nabla\phi \cdot n = 0 \quad \text{on} \quad \Gamma. \tag{6c}$$

The staggered approach first solves the displacement and temperature fields for the fixed phase-field variable. The equilibrium of the displacement and temperature at time step $i+1$ is ensured by convergence criteria as

$$\mathrm{err} = \max\left(\frac{\|\boldsymbol{u}_{i+1} - \boldsymbol{u}_i\|_2}{\|\boldsymbol{u}_{i+1}\|_2}, \frac{\|T_{i+1} - T_i\|_2}{\|T_{i+1}\|_2}\right) \leq \mathrm{tol}, \tag{7}$$

where tol represents the user-defined tolerance, with a specific value of $\mathrm{tol} = 1\times10^{-5}$ chosen for this work. Once the aforementioned convergence criteria are satisfied, the phase-field equation is iteratively solved for the frozen displacement and thermal field. These equations are repeatedly solved within the same step until the equilibrium of all field variables is achieved (refer to Algorithm 1 for more detailed information). The convergence criteria with three fields i.e., displacement, temperature, and phase-field are defined as follows:

$$\mathrm{err} = \left(\frac{\|\boldsymbol{u}_{i+1} - \boldsymbol{u}_i\|_2}{\|\boldsymbol{u}_{i+1}\|_2}, \frac{\|T_{i+1} - T_i\|_2}{\|T_{i+1}\|_2}, \frac{\|\phi_{i+1} - \phi_i\|_2}{\|\phi_{i+1}\|_2}\right) \leq \mathrm{tol}. \tag{8}$$

3. Fenics implementation

In this work, we utilize FEniCS [40], an open-source finite element package, to solve coupled differential equations Eqs. (1), (2) and (5). FEniCS provides a convenient framework for efficiently translating scientific models into finite element code. The

Algorithm 1: Staggered solution algorithm for adaptive PFM for thermal fracture.

Initialize at step (i): For a given mesh discretization, $\boldsymbol{u}_i$, T_i, ϕ_i and H_i^+, $\tilde{u} = \Delta u$
for every time step, i **do**
  while $||\boldsymbol{u}_{i+1} - \boldsymbol{u}_i||_2/||\boldsymbol{u}_{i+1}||_2$ *and* $||T_{i+1} - T_i||_2/||T_{i+1}||_2 \geq$ tolerance **do**
    Compute displacement field ($\boldsymbol{u}_{i+1}^h$)
    Compute temperature field (T_{i+1})
    Compute $\psi_0^{\mathrm{el}^{\pm}}$
    while $||\boldsymbol{u}_{i+1} - \boldsymbol{u}_i||_2/||\boldsymbol{u}_{i+1}||_2$ *and* $||T_{i+1} - T_i||_2/||T_{i+1}||_2$ *and* $||\phi_{i+1} - \phi_i||_2/||\phi_{i+1}||_2$ **do**
      Compute phase-field variable (ϕ_{i+1})
      if *RefineNeeded()* **then**
        Update mesh and variational form.
      end
    end
    Update history variable (H^+)
  end
end

computational capabilities of this open-source platform have been extensively investigated in the context of the PFM [39,45]. However, these implementations primarily utilize uniformly refined discretization or pre-defined locally refined discretization. In this work, we extend the implementation (FEniCS (*Dolfin version 2019.1*)) with an adaptive refinement strategy to numerically solve the discretized formulation of the governing equations Eqs. (1), (2) and (5) of the PFM that serves as the building block of the present work. Moreover, we investigate the feasibility of the error indicator in the presence of the thermal field, exploring its potential applications.

At the beginning of the simulation, the displacement, temperature, and phase-field are computed on the initial coarse mesh, which is generated using Gmsh [46] and converted to *.xml* format with "*dolfin-convert inputmesh.msh outputmesh.xml*" command. The initial configuration is depicted in Fig. 2a. Additionally, a known length scale parameter, ℓ_0 is set. Then, the error indicator based on the strain energy and the phase-field variable identifies the areas to be refined further, which is given as

$$\eta = (\Psi_i^{\mathrm{ele}} - \Psi_{i-1}^{\mathrm{ele}}), \text{ and } \phi \geq 0.25, \tag{9}$$

where η : elements need to refine further, $\Psi_i^{\mathrm{ele}} = \int_{\mathrm{ele}}(2\phi - 2)H^+$: integral of the crack driving force at step i, and $\Psi_{i-1}^{\mathrm{ele}}$: integral of the crack driving force at step $i-1$. The identified region is then locally refined as shown in Fig. 2b, and Fig. 2c. This is simple to accomplish with the help of the built-in FEniCS key *refine* (see Appendix Listing 1 for FEniCS implementation details). To restrict the infinite refinement of an element, we further check if the minimum element size satisfies the constraint $h \leq \ell/2$. The element with satisfying criteria is removed from the list of elements to be refined as illustrated in Fig. 2d (see Appendix Listing 1 for FEniCS implementation details).

The known solutions and variational forms are updated after the refinement of the mesh. Please refer to Appendix for more details.

4. Results and discussion

This section presents the results obtained from the adaptive PFM implementation in FEniCS for thermal cracking. Several boundary value problems are considered to demonstrate different characteristics of the cracking due to thermo-mechanical interactions, including crack nucleation, propagation, and crack curving. These fracture problems will demonstrate the effectiveness of the implemented adaptive PFM in handling a wide range of thermal fracture scenarios.

4.1. Cruciform specimen

To validate our FEniCS implementation, we first perform a benchmark by applying the code to a well-established standard problem: A cruciform specimen with an initial crack of size a. This standard problem is introduced by Prasad et al. [47] and further investigated by other researchers [48–50]. In this problem, a cruciform domain (initially kept as $T_0 = 0°$) with a corner crack as shown in Fig. 3 is used to solve for various mechanical and thermal boundary conditions. In the cruciform specimen, the left and right edge of the specimen is restrained to move in $x-$direction while the bottom edge is constrained to move in $y-$direction. The interactions of the thermal and mechanical boundary conditions are investigated through two test cases presented in Table 1, depending upon the specific boundary conditions applied.

Following the work of Mandal et al. [50], the material properties are chosen as, Young's modulus, $E = 218.4\,\mathrm{GPa}$, Poisson's ratio, $\nu = 0.2$, critical fracture toughness, $\mathcal{G}_c = 2 \times 10^{-4}\,\mathrm{J\,m^{-2}}$, density, $\rho = 2450\,\mathrm{kg\,m^{-3}}$, thermal conductivity, $k = 1.0\,\mathrm{W\,m^{-1}\,K^{-1}}$, specific heat at constant pressure, $C_p = 1.0\,\mathrm{J\,kg^{-1}\,K^{-1}}$, coefficient of thermal expansion, $\alpha = 6 \times 10^{-4}\,\mathrm{K^{-1}}$. The simulation starts with a coarse mesh with 17100 linear triangular elements, and the length scale parameter is chosen as $\ell_0 = 0.025 \times 10^{-3}\,\mathrm{mm}$.

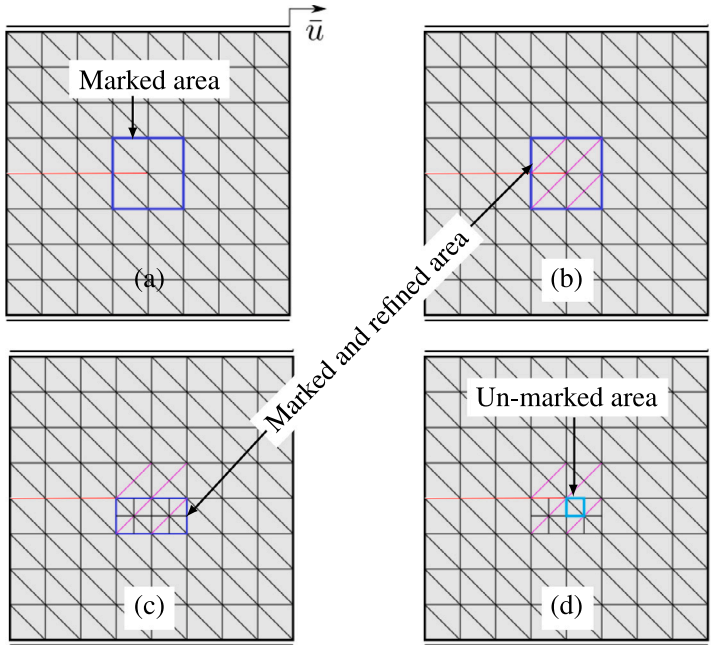

Fig. 2. Schematic representation of adaptive mesh refinement scheme for a load-step (a) identity for the refinement using error indicator, (b) refine using FEniCS in-built "refine" command, (c) refine again if $h \leq \ell_0/2$, and (d) un-mark area for the refinement if $\ell_0 \leq 2h$.

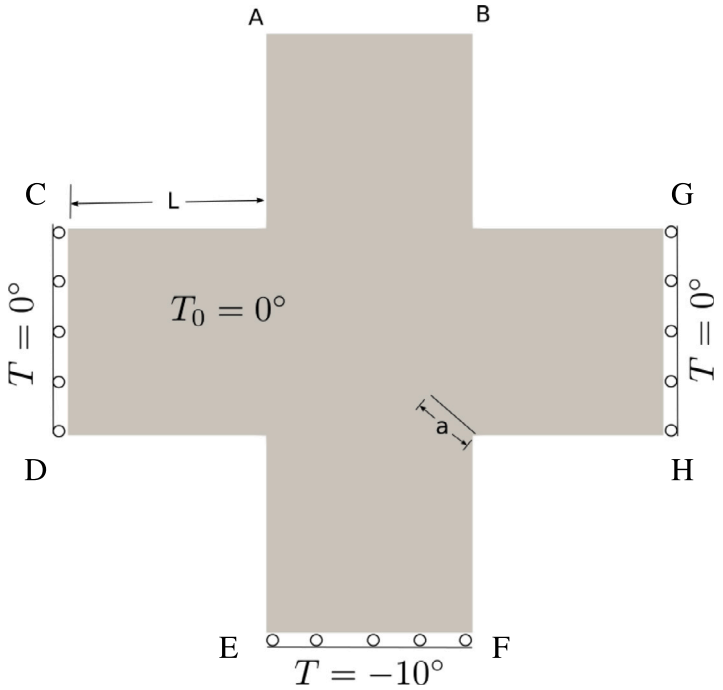

Fig. 3. Cruciform specimen: Domain and the boundary conditions. Here, the crack is geometry induced and the ratio of a/L = 0.2, and the angle between the crack and vertical axis is 45°.

Table 1
Cruciform specimen: two cases based on the application of boundary conditions on Edge AB (see, Fig. 3).

Case	Temperature (°C)				Displacement (mm)
	AB	CD	EF	GH	AB (y–direction)
case: I	10	0	−10	0	–
case: II	10	0	−10	0	0.1

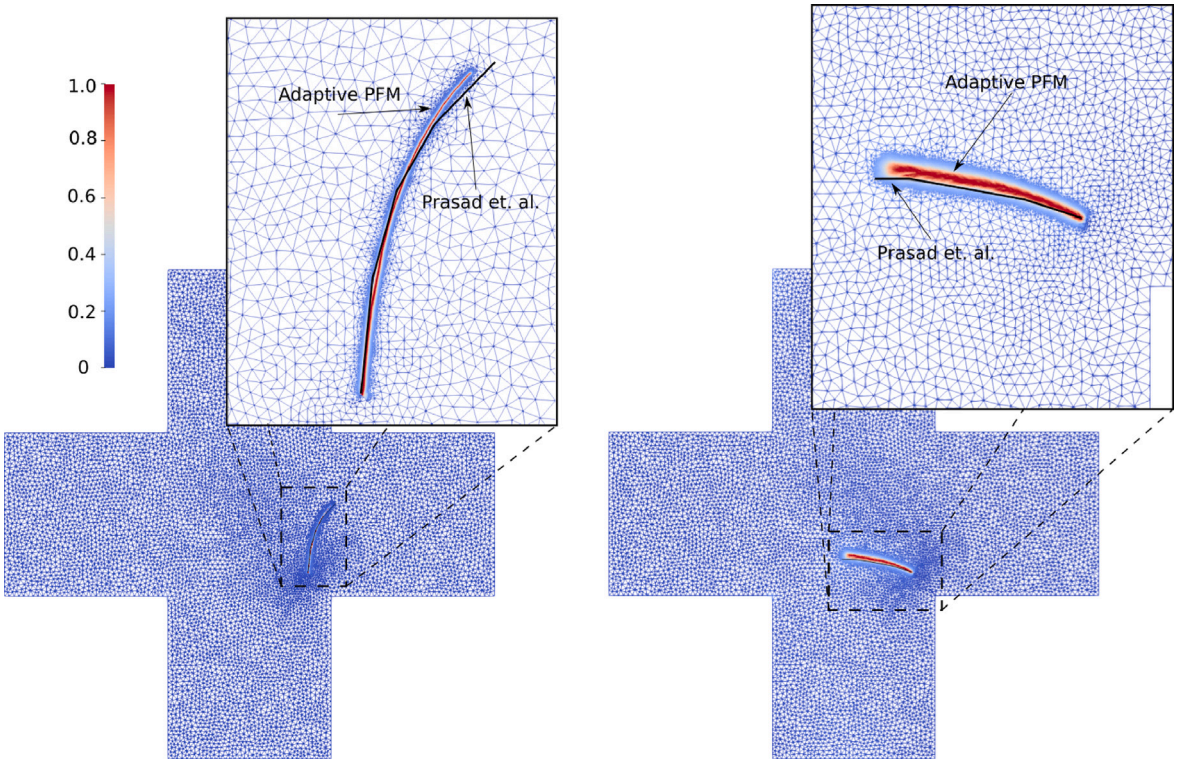

Fig. 4. Cruciform specimen: Crack trajectory for case: I and case: II compared against Prasad et al. [47].

As the simulation progresses, the proposed scheme dynamically identifies and refines the domain's crucial areas within the domain. The adaptive refinement process facilitates the accurate tracing of the crack trajectory in an automatic manner. The crack trajectory for different cases obtained using proposed adaptive PFM and from other methods are shown in Fig. 4. In case I, the crack propagates slightly vertically and then bends along a curved path towards the right. In case II, the crack propagates horizontally while following the curve trajectory. These results demonstrate that the proposed adaptive PFM is capable of capturing different cracking mechanisms arising from thermo-mechanical interactions. However, there is a slight deviation in the crack trajectory compared to the results obtained using the boundary element method in the literature [47]. This discrepancy may be attributed to the numerical errors associated with different numerical approaches employed in the literature [50]. The corresponding temperature profile is shown in Fig. 5, which is consistent with the results reported by Wang [51]. These test cases highlight the intricate interplay between the thermal and mechanical aspects of the problem of material damage due to thermo-mechanical interactions.

4.2. Quench test

We now examine the quenching behavior of a ceramic slab at three different initial temperatures: 550 K, 680 K, and 980 K. The ceramic slab is cooled by immersing it in a medium at an ambient temperature of 300 K. Considering the symmetry of the slab, only one-quarter of the entire ceramic slab is simulated, as illustrated in Fig. 6. Specific boundary conditions are applied to account for the symmetry. The symmetry boundary condition is imposed at the top and the left edges, constraining the right edge to move in x–direction and restricting the displacement in y–displacement at the top edge. On the other hand, at the bottom and left edges, the Dirichlet boundary condition for the temperature is imposed, setting T_{ref} =300 K.

Following the work of Wang et al. [52], the material properties are chosen as Young's modulus, E = 340 GPa, Poisson's ratio, ν = 0.22, critical fracture toughness, $\mathcal{G}_c$ = 42.47 J m^{-2}, density, ρ = 2450 kg m^{-3}, thermal conductivity, k = 300 W m^{-1} K^{-1}, specific

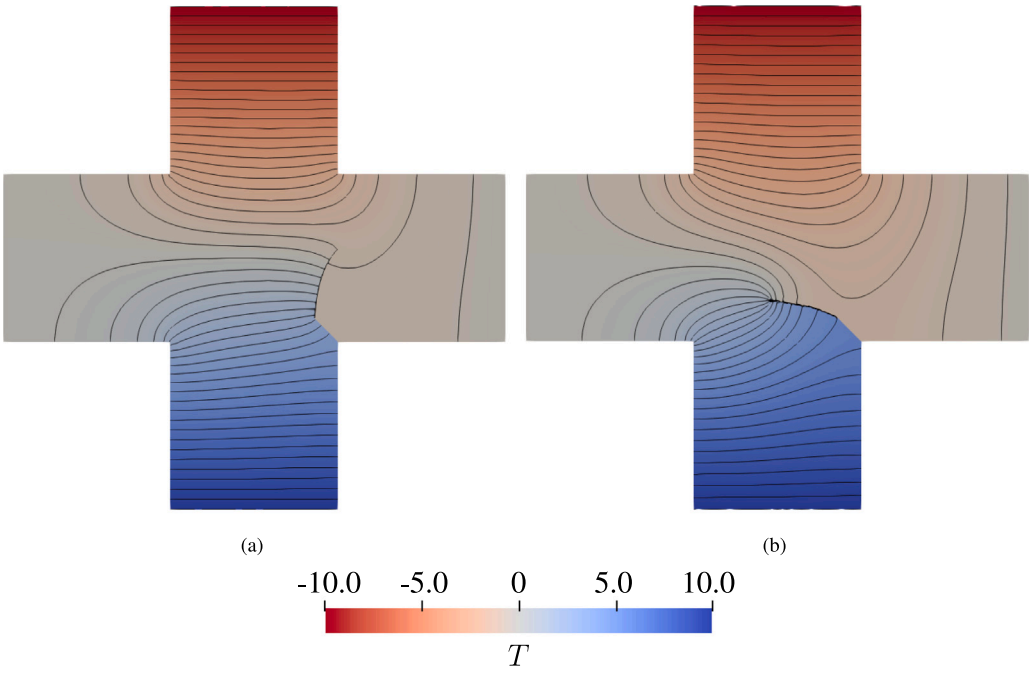

Fig. 5. Cruciform specimen: Temperature contour for (a) case I, (b) case: II.

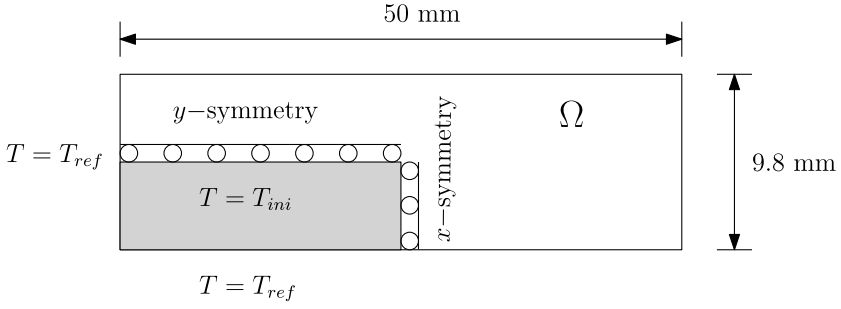

Fig. 6. Quench test: domain and the boundary conditions.

heat at constant pressure, $C_p = 0.775\,\mathrm{J\,kg^{-1}\,K^{-1}}$, coefficient of thermal expansion, $\alpha = 8.0 \times 10^{-6}\,\mathrm{K^{-1}}$. The characteristic length scale parameter, $\ell_0 = 0.06\,\mathrm{mm}$, and the time step $\Delta t = 1 \times 10^{-8}\,\mathrm{s}$ are set for the transient thermal problem.

At the beginning of the simulation, uniform damage is observed at the edges. As the simulation time increases, the uniform damage is localized to form small cracks. These small cracks further propagate, resulting from the large temperature gradient. It is worth noting that some cracks stop propagating. This is due to the insufficient supply of the strain energy. These observations agree well with the experimental [54] and simulation results reported in the literature [50,52]. Moreover, the proposed adaptive PFM automatically tracks the propagation of crack nucleation, crack arrest, and crack due to multi-physical interactions.

Next, we explore the influence of thermal gradient on crack propagation mechanisms. The thermal gradient is varied by altering the initial temperature of the ceramic slab. Fig. 7 shows the crack trajectories for the specimen with different initial temperatures. The crack pattern becomes denser as the thermal gradient ΔT increases. This phenomenon can be attributed to the elevated strain energy from the more considerable temperature difference. These findings align with experimental observations reported by Wang et al. [51] and Chu et al. [55], validating the impact of the thermal gradient on crack propagation behavior.

The simulation commences with 8,000 linear triangular elements. As the simulation time progresses, the adaptive refinement scheme automatically refines the regions around the crack trajectory, adjusting the number of elements based on the temperature variations ΔT. Fig. 8 shows the variation of a number of elements as a function of simulation time. After $t = 10\,\mu\mathrm{s}$, the domain is discretized with 37588, 43990, and 51863 elements for $\Delta T = 250\,\mathrm{K}$, $380\,\mathrm{K}$ and $580\,\mathrm{K}$, respectively. However, Li et al. [56] used 113152 Q4 elements for the uniform discretization and 52672, 61322, and 71328 quadtree elements with adaptive refinement for $\Delta T = 250\,\mathrm{K}$, $380\,\mathrm{K}$ and $580\,\mathrm{K}$, respectively. Furthermore, mesh discretization closely tracks the trajectories of crack propagation, dynamically refining the domain as the crack extends. This adaptive refinement approach ensures that the mesh resolution is

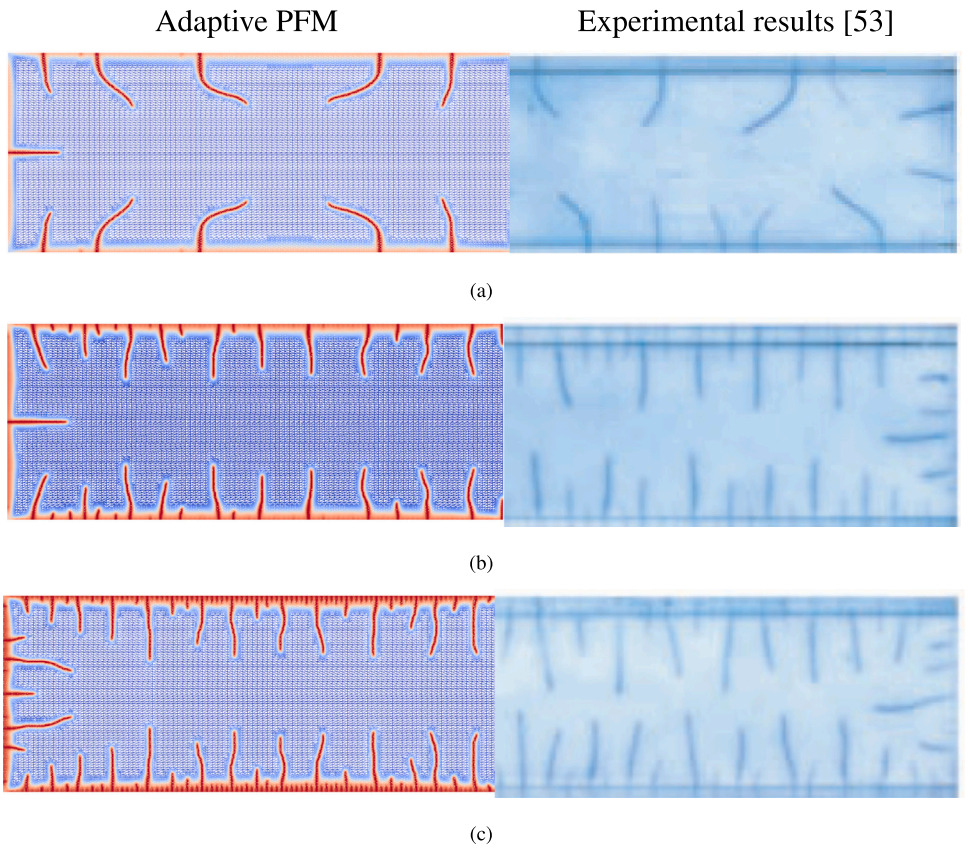

Fig. 7. Effect of temperature difference, ΔT on the crack growth (a) $\Delta T = 250\,\mathrm{K}$, (b) $\Delta T = 380\,\mathrm{K}$, and (c) $\Delta T = 580\,\mathrm{K}$ [53].

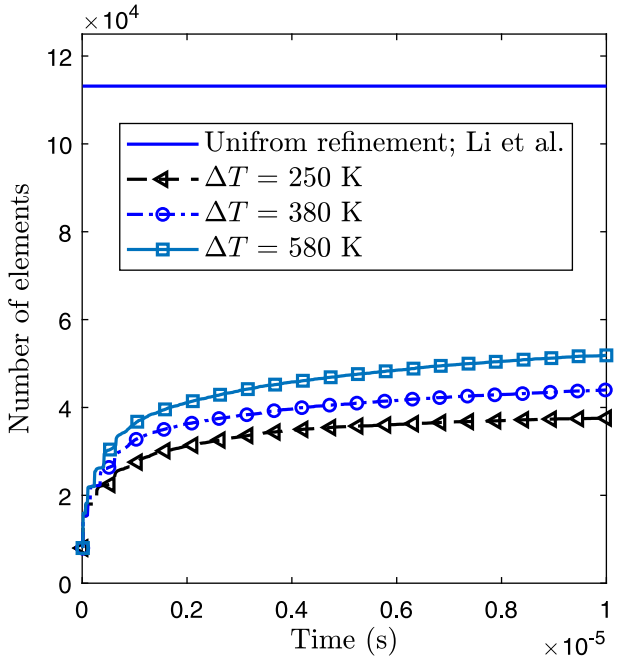

Fig. 8. Quench test: number of elements as a function of time increment. The adaptive PFM refinement results are compared against uniformly refined mesh reported by Li et al. [56], which requires 113152 Q4 elements.

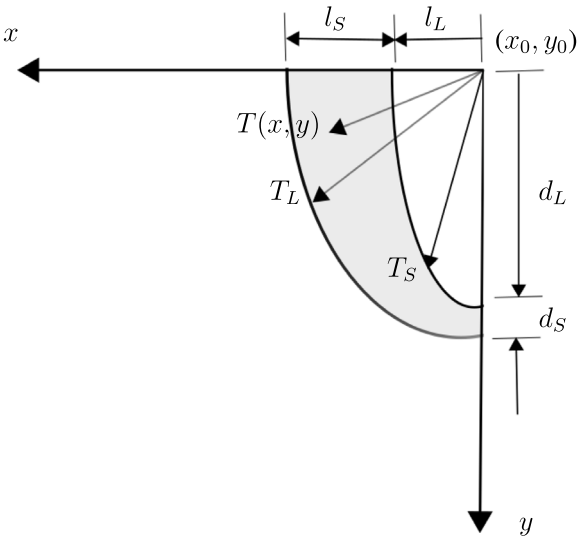

Fig. 9. Schematic representation of the analytical temperature profile. Here, T_L : liquids temperature, T_S : solidus temperature, (l_s, l_L) and (d_L, d_S) are the length and depth parameters corresponding to the liquids and solidus.

optimized to capture the evolving crack geometry accurately. It is important to note that the above examples assume homogeneous material properties. However, the FEniCS framework can also accommodate heterogeneous material properties or variations in material properties with temperature. The following section discusses the framework's effectiveness in handling such scenarios, specifically by investigating hot cracking during additive manufacturing.

4.3. Hot cracking in additive manufacturing

We extend the proposed framework to simulate the occurrence of hot cracking in additive manufacturing (AM), in which the fracture toughness and the coefficient of the thermal expansion vary as a function of temperature. In the context of AM, hot cracking refers to the formation of cracks in and around the melting pool. In this work, an analytical elliptic solution of the temperature in the vicinity of the melt pool is applied as shown in Fig. 9. A specific point at the ellipse contour is given in the polar coordinate as,

$$r = \sqrt{x^2 + y^2}, \quad \theta = \tan^{-1}|\frac{y - y_0}{x - x_0}|, \tag{10}$$

where r is the distance of the point to the ellipse's center (x_0, y_0), and θ is the angle from the top surface to the current position. The temperature field is calculated as,

$$T(x, y) = T(r, \theta) = T_L + c(T_L - T_S)\frac{r - r_L(\theta)}{r_S(\theta) - r_L(\theta)}, \tag{11}$$

where $r_L(\theta)$ and $r_S(\theta)$ represents isolines of $T = T_L$ and $T = T_S$, respectively. The radii for the liquids and solidus are given as [24],

$$r_L(\theta) = \sqrt{\frac{(l_L d_L)^2}{(d_L cos(\theta))^2 + (l_L sin(\theta))^2}}, \tag{12}$$

$$r_S(\theta) = \sqrt{\frac{(l_S d_S)^2}{(d_S cos(\theta))^2 + (l_S sin(\theta))^2}}, \tag{13}$$

Here, the length parameters (l_L, l_S) and the depth parameters (d_L, d_S) correspond to liquids and solidus, respectively.

In this work, the solidification shrinkage strain ϵ_{ss} is simulated using the effective thermal expansion coefficient $\bar{\alpha}(T)$. For alloys, solidification happens once the liquid in the melting pool region reaches the solidus temperature T_S. The subsequent shrinkage of the solidifying solid is proportional to the change of solid fraction. Here, we assume that the effective thermal expansion coefficient takes the following form:

$$\bar{\alpha}(T) = \begin{cases} \alpha_T, & T < T_S, \\ \alpha_T + \alpha_{SS}, & T_S \leq T \leq T_L, \\ \alpha_T, & T_L < T, \end{cases} \tag{14}$$

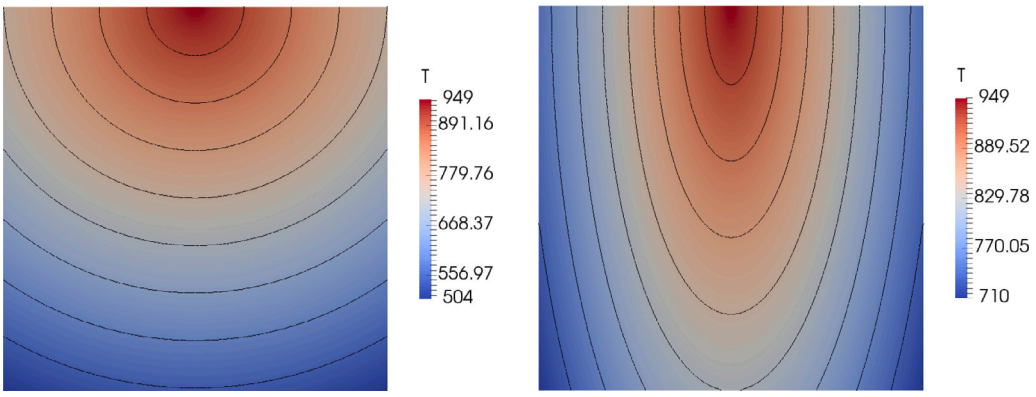

(a) (b)

Fig. 10. Analytical temperature profile for the different aspect ratio (a) 1, and (b) 3.

where $\alpha_{SS} = \dfrac{\epsilon_{SS}}{T_L - T_S}$. Correspondingly, the thermal strain can be written as,

$$\epsilon_T = \tilde{\alpha}(T)(T - T_0) = \begin{cases} \alpha_T(T - T_0), & T < T_S, \\ \alpha_T(T - T_0) + \alpha_{SS}(T - T_S), & T_S \le T < T_L, \\ \alpha_T(T_L - T_0) + \alpha_{SS}(T_L - T_S), & T_L \le T, \end{cases} \tag{15}$$

Additionally, the crack onset for the non-isothermal brittle fracture is affected by the temperature dependency of fracture toughness. Hence in this work, the temperature dependency of fracture toughness is considered as,

$$\mathcal{G}_c = \mathcal{G}_{c0}\left(1 - b_1\left(\frac{T - T_{\text{ref}}}{T_{\max}}\right) + b_2\left(\frac{T - T_{\text{ref}}}{T_{\max}}\right)^2\right), \tag{16}$$

where b_1 and b_2 are the model parameter constants, $\mathcal{G}_c$ is the effective fracture toughness, $\mathcal{G}_{c0}$ is the fracture toughness at reference temperature T_{ref} and $T_{\max}$ maximum temperature.

Now, we consider a two-dimensional plane strain domain with a cross-section of 10 mm X 10 mm. The simulation parameters for AM specimen are set as, $T_S = 900\,\text{K}$, $T_L = 890\,\text{K}$, $l_L = 3.5$, $l_S = 4.0$, $d_L = 7.0 \times a$, and $d_S = 8.0 \times a$, where $a = 1, 3$ is the aspect ratio. Fig. 10 displays the analytical temperature profiles for the different aspect ratios $a = 1, 3$. The melt pool is small for the lower aspect ratio and deeper for the larger aspect ratio, which is apparent from the analytical temperature contour profile.

To begin, we analyze the problem using a uniform mesh discretization. The simulation results reveal the formation of a circumferential crack pattern within the temperature ranges of the liquidus and solidus (as depicted in Figs. 11a and 11b). This crack pattern emerges due to the generation of solidification shrinkage strain resulting from the phase transformation within the liquidus and solidus regions. Subsequently, we employ a very coarse mesh discretization in combination with an adaptive refinement strategy to simulate the same phenomena in AM. The crack trajectory and adaptively refined mesh are depicted in Fig. 12. Both the adaptive approach and the PFM with uniformly refined mesh accurately reproduce the experimental crack trajectory. However, the adaptive PFM requires a lesser number of elements to capture the length scale characteristic as compared to the uniformly refined mesh. This clearly demonstrates the significant computational savings achieved when solving the coupled differential equations and storing the data. As the cracks in additive manufacturing processes tend to nucleate in localized regions, the adaptive approach proves to be an efficient and practical solution. The adaptive approach is well-suited for simulating hot cracking in additive manufacturing by reducing computational effort and minimizing data storage requirements.

One of the added advantages of using FEniCS is the simplicity of the extension from the two-dimensional models to the three-dimensional model. The transition from a two-dimensional model to a three-dimensional model in FEniCS involves a straightforward modification i.e., adding a third dimension when generating the domain discretization using Gmsh. The code structure and implementation mostly remain unchanged as illustrated in code Appendix listing 3. In order to demonstrate this advantage, we now consider a three-dimensional domain (10 mm x 10 mm x 0.1 mm). In the three-dimensional problem, the bottom edge is restricted to move exclusively in the $y-$ direction, while the bottom end node is constrained to move in both the $x-$ and $z-$ directions. The crack trajectory in a thin three-dimensional layer for aspect ratios of 1 and 3, which is consistent with the two-dimensional problem, is depicted in Fig. 13. These results highlight how the crack propagates in three-dimensional space, demonstrating the extension of the crack trajectory behavior from the two-dimensional problem to the three-dimensional case.

5. Concluding remarks and future outlook

In this work, we have proposed a straightforward concept to enable adaptive numerical solution schemes for PFM to simulate thermal fracture. The error estimator for the adaptive mesh refinement is based on the combination of strain energy density, ψ, and

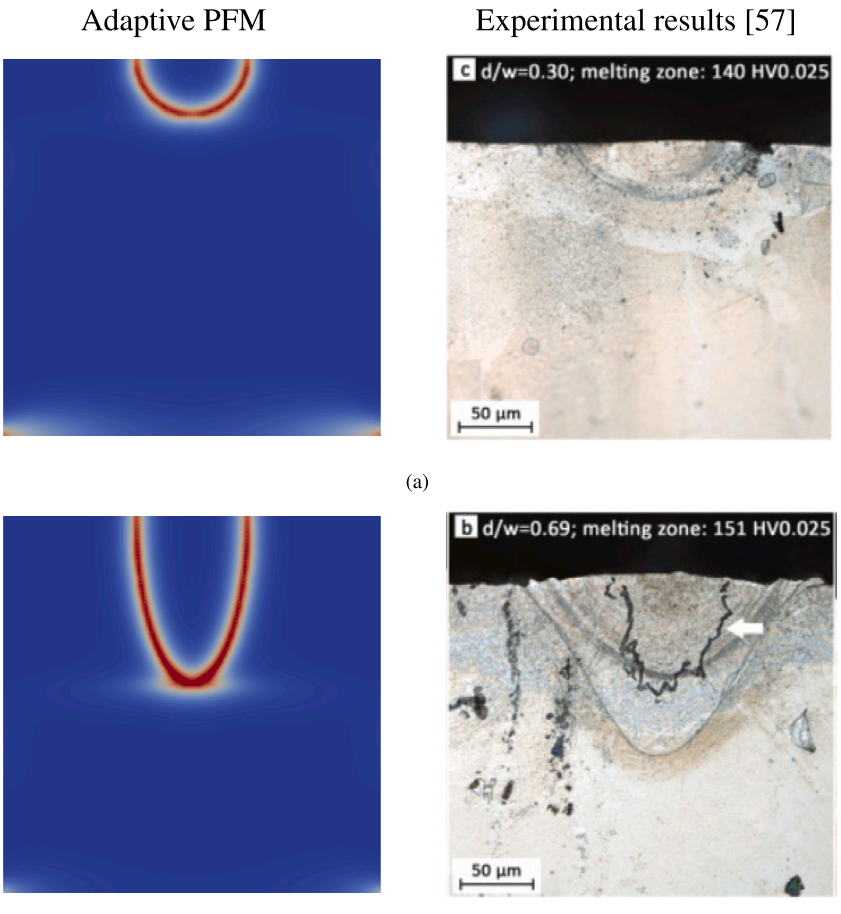

Fig. 11. Circumferential cracking of the melt pool during AM for aspect ratio (a) $a = 1$ and (b) $a = 3$ [57].

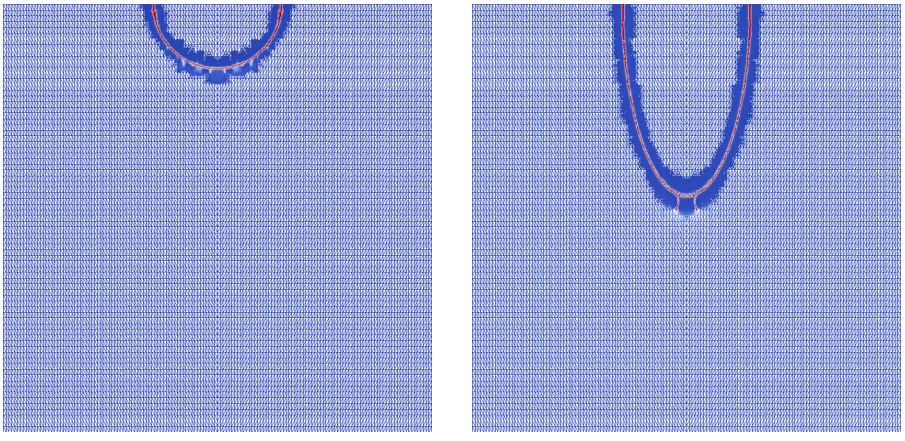

Fig. 12. Adaptive discretization and crack profile for aspect ratio (a) $a = 1$ and (b) $a = 3$.

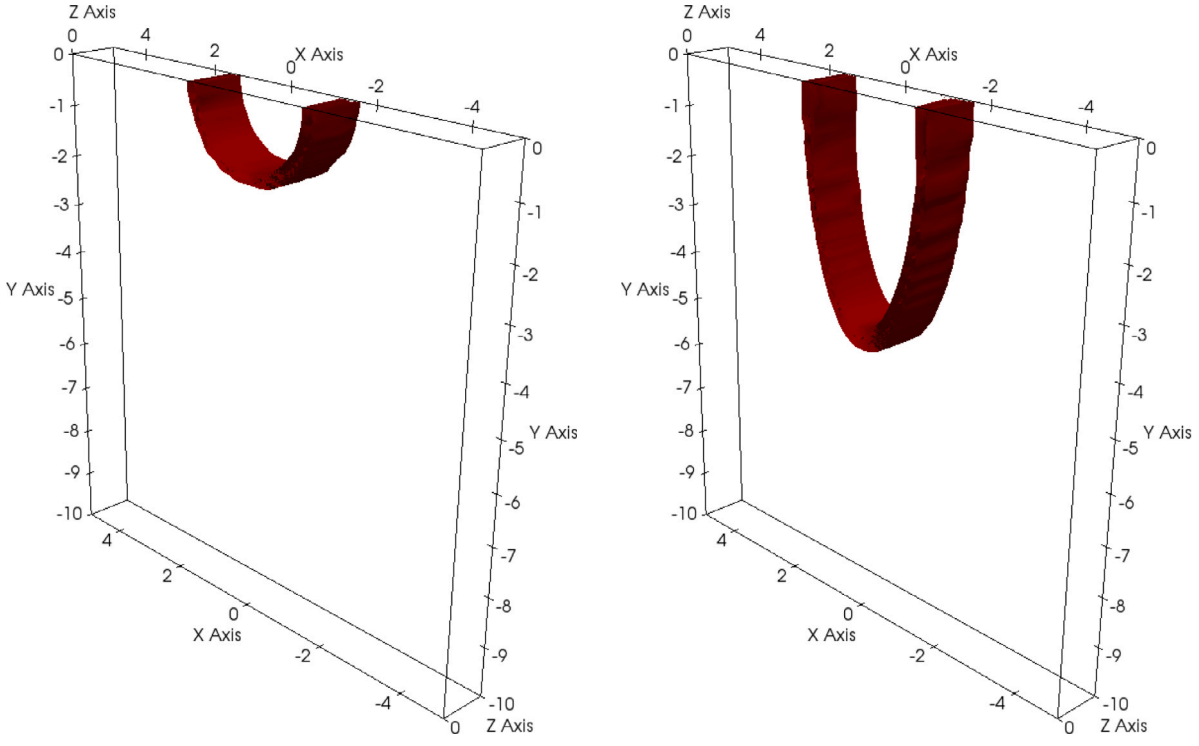

Fig. 13. Three-dimensional crack trajectory for aspect ratio (a) $a = 1$, and (b) $a = 3$.

phase-field variable, ϕ. The proposed framework is implemented in an open-source finite element method, FEniCS [40] for both two and three dimensions due to its robustness and ease of implementation. The robustness of the framework and the efficacy of the implementation are demonstrated with complex examples involving fracture due to coupled interaction (thermal quenching and hot cracking in AM). The results obtained using the proposed adaptive PFM demonstrate a high level of accuracy in reproducing the findings from the uniform mesh approach as well as the numerical and experimental results reported in the literature. The main observations are as follows:

- Adaptive PFM automatically traces the propagating crack trajectories, requiring fewer elements than PFM with uniformly refined mesh.
- The proposed framework can simulate crack nucleation and crack formation with curve trajectory.
- The crack pattern becomes denser for a higher thermal gradient which is consistent with experimental observations.
- The shallow and key-hole mode fracture in AM can be simulated with the application of analytical temperature profiles with different aspect ratios.

The current implementation could be used as an efficient computational tool to model fracture problems with different multi-physical interactions such as hydrogen embrittlement, fracture in Li-ion battery particles, and stress corrosion cracking. Although the current implementation has considered only the quadratic degradation function, the proposed approach can easily be extended to other phase field models, such as the phase field regularized cohesive zone model and other degradation functions.

CRediT authorship contribution statement

Hirshikesh: Writing – original draft, Visualization, Validation, Software, Methodology, Investigation, Conceptualization. **Daniel Schneider:** Writing – review & editing, Supervision, Resources, Project administration, Methodology, Conceptualization. **Britta Nestler:** Writing – review & editing, Supervision, Project administration, Funding acquisition, Conceptualization.

Declaration of competing interest

The authors declare the following financial interests/personal relationships which may be considered as potential competing interests: Britta Nestler reports financial support was provided by Helmholtz association.

Data availability

Data will be made available on request.

Acknowledgments

The authors gratefully acknowledge the financial support by the Helmholtz association, Germany through the program "Material System Engineering (MSE)" (no. 43.31.01).

Appendix. FEniCS implementation of adaptive refinement strategies

```
def RefineIfNeeded():
    global mesh
    CM =  MeshFunction("bool", mesh, mesh.topology().dim())
    for cell in cells(mesh):
        mid = cell.midpoint()
        if cell.h() > lc/2.0 and phi(mid) > 1/4:
            CM[cell] = True
        else:
            CM[cell] = False
    mesh = refine(mesh, CM)
    SetSpaces(True)
```

Listing 1: Identifying domain to be refined and refinement of the domain.

For the adaptive mesh refinement strategy, the known solution and the variational forms have to be updated after mesh refinement. The interpolation of the coarse mesh solution on the corresponding refined mesh is achieved using the built-in function key "project". Fig. A.14a shows the temperature field on a coarse mesh. The known solution on the coarse mesh is interpolated on the updated, refined mesh as shown in Fig. A.14b. It is worth noting that this approach works on jobs running in serial as well as parallel. Listing 2 presents a simple code for updating the evolution equation after mesh refinement. Similarly, all the known fields and variational forms for the temperature and displacement can be updated.

```
def SetSpaces(Update = False):
    global mesh, l, ds
    global FS_phi, Solver_phi, HistUpdate, phi, PhiNew, PhiOld

    if Update:
        phi_, PhiNew_, PhiOld_, HistUpdate_ = phi, PhiNew, PhiOld, HistUpdate

    FS_phi = FunctionSpace(mesh,'CG',1)
    facets = MeshFunction("size_t", mesh, 1)
    facets.set_all(0)
    Left().mark(facets, 1)
    Right().mark(facets,2)
    Bottom().mark(facets,3)
    Top().mark(facets,4)
    bc_phi = []
    W = FunctionSpace(mesh, 'DG', 0)
    HistUpdate = Function(W)
    ds = Measure('ds', subdomain_data=facets)
    PhiTrial, PhiTest = TrialFunction(FS_phi), TestFunction(FS_phi)
    phi = Function(FS_phi)

    if Update:
        phi.assign(project(phi_, FS_phi))
        PhiOld.assign(PhiOld_), HistUpdate.assign(HistUpdate_)

    E_phi = (Gc*l*inner(grad(PhiTrial),grad(PhiTest))+((Gc/l)+\
  2.0*HistUpdate)*inner(PhiTrial,PhiTest)- 2.0*HistUpdate*PhiTest)*dx
   problem_phi = LinearVariationalProblem(lhs(E_phi), rhs(E_phi), phi)
    solver_phi = LinearVariationalSolver(problem_phi)
```

Listing 2: Update functions, and variational form for current mesh.

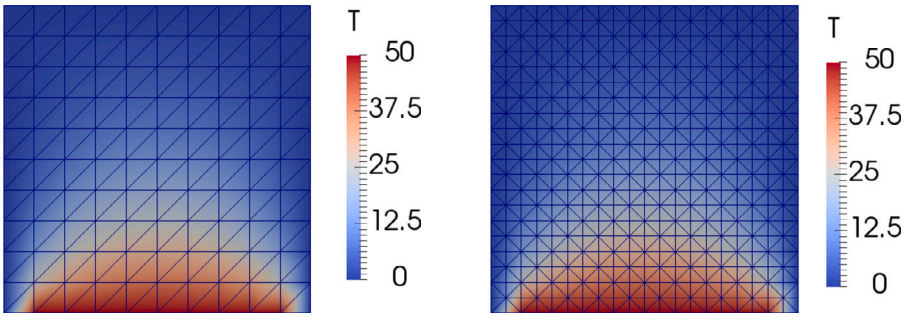

Fig. A.14. Projection of the coarse mesh solution on the updated, refined mesh (a) temperature field on coarse mesh, and (b) temperature field projected on the refined mesh.

```python
def epsilon(v):
    return sym(grad(v))
def sigma(u, phi_old):
    return (pow((1.0 - phi_old),2) + k)*(2.0*mu*epsilon(u) +lmbda*tr(epsilon(u))*Identity(ndim))
# Note here ndim is the dimension of the problem.
```

Listing 3: Python code to compute strain and stress for three dimensions

References

[1] Gallina Davide. Finite element prediction of crack formation induced by quenching in a forged valve. Eng Fail Anal 2011;18:2250–9.

[2] Chen Yuan, Lu Fenggui, Zhang Ke, Nie Pulin, Hosseini Seyed Reza Elmi, Feng Kai, et al. Dendritic microstructure and hot cracking of laser additive manufactured Inconel 718 under improved base cooling. J Alloys Compd 2016;670:312–21.

[3] Smith PK, Baxter CA. Fracture during cooling of cast borosilicate glass containing nuclear wastes. 1981.

[4] Wu Shibo, Lei Zhenglong, Li Bingwei, Liang Jingwei, Chen Yanbin. Hot cracking evolution and formation mechanism in 2195 Al-Li alloy printed by laser powder bed fusion. Addit Manuf 2022;54:102762.

[5] Chauvet Edouard, Kontis Paraskevas, Jägle Eric A, Gault Baptiste, Raabe Dierk, Tassin Catherine, et al. Hot cracking mechanism affecting a non-weldable Ni-based superalloy produced by selective electron beam melting. Acta Mater 2018;142:82–94.

[6] Lu Nannan, Lei Zhenglong, Hu Kuan, Yu Xingfu, Li Peng, Bi Jiang, et al. Hot cracking behavior and mechanism of a third-generation Ni-based single-crystal superalloy during directed energy deposition. Addit Manuf 2020;34:101228.

[7] Bayat Seyed Hadi, Nazari Mohammad Bagher. Thermal fracture analysis in orthotropic materials by XFEM. Theor Appl Fract Mech 2021;112:102843.

[8] Chadaram Srinivasu, Yadav Saurabh Kumar. Three-dimensional thermal fracture analysis of piezoelectric material by extended finite element methods. Eng Fract Mech 2021;256:107981.

[9] Feulvarch Eric, Fontaine Mickael, Bergheau Jean-Michel. XFEM investigation of a crack path in residual stresses resulting from quenching. Finite Elem Anal Des 2013;75:62–70.

[10] Bouchard PO, Bay F, Chastel Y. Numerical modelling of crack propagation: Automatic remeshing and comparison of different criteria. Comput Methods Appl Mech Engrg 2003;192(35):3887–908.

[11] Bourdin B, Francfort GA, Marigo JJ. Numerical experiments in revisited brittle fracture. J Mech Phys Solids 2000;48(4):797–826.

[12] Borden Michael J, Verhoosel Clemens V, Scott Michael A, Hughes Thomas JR, Landis Chad M. A phase-field description of dynamic brittle fracture. Comput Methods Appl Mech Engrg 2012;217:77–95.

[13] Schlüter Alexander, Willenbücher Adrian, Kuhn Charlotte, Müller Ralf. Phase field approximation of dynamic brittle fracture. Comput Mech 2014;54(5):1141–61.

[14] Nguyen TT, Yvonnet J, Zhu Q-Z, Bornert M, Chateau C. A phase-field method for computational modeling of interfacial damage interacting with crack propagation in realistic microstructures obtained by microtomography. Comput Methods Appl Mech Engrg 2016;312:567–95.

[15] Raina Arun, Miehe Christian. A phase-field model for fracture in biological tissues. Biomech Model Mechanobiol 2016;15(3):479–96.

[16] Msekh Mohammed A, Cuong NH, Zi G, Areias P, Zhuang X, Rabczuk Timon. Fracture properties prediction of clay/epoxy nanocomposites with interphase zones using a phase field model. Eng Fract Mech 2018;188:287–99.

[17] Hirshikesh, Natarajan Sundararajan, Annabattula Ratna Kumar. Modeling crack propagation in variable stiffness composite laminates using the phase field method. Compos Struct 2019;209:424–33.

[18] Lo Yu-Sheng, Borden Michael J, Ravi-Chandar K, Landis Chad M. A phase-field model for fatigue crack growth. J Mech Phys Solids 2019;132:103684.

[19] Li Peidong, Li Weidong, Li Biao, Yang Shuo, Shen Yongxing, Wang Qingyuan, et al. A review on phase field models for fracture and fatigue. Eng Fract Mech 2023;289:109419.

[20] Miehe C, Welschinger F, Hofacker M. Thermodynamically consistent phase-field models of fracture: Variational principles and multi-field FE implementations. Internat J Numer Methods Engrg 2010;83:1273–311.

[21] Miehe Christian, Schänzel Lisa-Marie, Ulmer Heike. Phase field modeling of fracture in multi-physics problems. Part I. Balance of crack surface and failure criteria for brittle crack propagation in thermo-elastic solids. Comput Methods Appl Mech Engrg 2015;294:449–85.

[22] Miehe C, Hofacker M, Schänzel L-M, Aldakheel F. Phase field modeling of fracture in multi-physics problems. Part II. coupled brittle-to-ductile failure criteria and crack propagation in thermo-elastic–plastic solids. Comput Methods Appl Mech Engrg 2015;294:486–522.

[23] Miehe Christian, Mauthe Steffen. Phase field modeling of fracture in multi-physics problems. Part III. Crack driving forces in hydro-poro-elasticity and hydraulic fracturing of fluid-saturated porous media. Comput Methods Appl Mech Engrg 2016;304:619–55.

[24] Ruan Hui, Rezaei Shahed, Yang Yangyiwei, Gross Dietmar, Xu Bai-Xiang. A thermo-mechanical phase-field fracture model: Application to hot cracking simulations in additive manufacturing. J Mech Phys Solids 2023;172:105169.
[25] Badnava Hojjat, Msekh Mohammed A, Etemadi Elahe, Rabczuk Timon. An h-adaptive thermo-mechanical phase field model for fracture. Finite Elem Anal Des 2018;138:31–47.
[26] Zhang Zhengru, Ma Yuan, Qiao Zhonghua. An adaptive time-stepping strategy for solving the phase field crystal model. J Comput Phys 2013;249:204–15.
[27] lin Liao Hong, Ji Bingquan, Zhang Luming. An adaptive BDF2 implicit time-stepping method for the phase field crystal model. IMA J Numer Anal 2022;42:649–79.
[28] Gupta Abhinav, Krishnan U Meenu, Chowdhury Rajib, Chakrabarti Anupam. An auto-adaptive sub-stepping algorithm for phase-field modeling of brittle fracture. Theor Appl Fract Mech 2020;108:102622.
[29] Heister Timo, Wheeler Mary F, Wick Thomas. A primal-dual active set method and predictor-corrector mesh adaptivity for computing fracture propagation using a phase-field approach. Comput Methods Appl Mech Engrg 2015;290:466–95.
[30] Areias P, Rabczuk T, Msekh MA. Phase-field analysis of finite-strain plates and shells including element subdivision. Comput Methods Appl Mech Engrg 2016;312(Supplement C):322–50.
[31] Burke S, Ortner C, Süli E. An adaptive finite element approximation of a variational model of brittle fracture. SIAM J Numer Anal 2010;48(3):980–1012.
[32] Welschinger Fabian, Hofacker Martina, Miehe Christian. Configurational-force-based adaptive FE solver for a phase field model of fracture. PAMM 2010;10(1):689–92.
[33] Hirshikesh, Jansari Chintan, Kannan K, Annabattula RK, Natarajan S. Adaptive phase field method for quasi-static brittle fracture using a recovery based error indicator and quadtree decomposition. Eng Fract Mech 2019;220:106599.
[34] Hirshikesh, Pramod ALN, Annabattula RK, Ooi ET, Song C, Natarajan S. Adaptive phase-field modeling of brittle fracture using the scaled boundary finite element method. Comput Methods Appl Mech Engrg 2019;355:284–307.
[35] Berger-Vergiat Luc, Waisman Haim. An overlapping domain decomposition preconditioning method for monolithic solution of shear bands. Comput Methods Appl Mech Engrg 2017;318:33–60.
[36] Svolos Lampros, Berger-Vergiat Luc, Waisman Haim. Updating strategy of a domain decomposition preconditioner for parallel solution of dynamic fracture problems. J Comput Phys 2020;422:109746.
[37] Jodlbauer D, Langer U, Wick T. Matrix-free multigrid solvers for phase-field fracture problems. Comput Methods Appl Mech Engrg 2020;372:113431.
[38] Storvik Erlend, Both Jakub Wiktor, Sargado Juan Michael, Nordbotten Jan Martin, Radu Florin Adrian. An accelerated staggered scheme for variational phase-field models of brittle fracture. Comput Methods Appl Mech Engrg 2021;381:113822.
[39] Hirshikesh, Natarajan Sundararajan, Annabattula Ratna Kumar. A FEniCS implementation of the phase field method for quasi-static brittle fracture. Front Struct Civ Eng 2019;13:380–96.
[40] Alnæs Martin S, Blechta Jan, Hake Johan, Johansson August, Kehlet Benjamin, Logg Anders, et al. The FEniCS project version 1.5. Arch Numer Softw 2015;3(100).
[41] Tangella Raja Gopal, Kumbhar Pramod, Annabattula Ratna Kumar. Hybrid phase-field modeling of thermo-elastic crack propagation. Int J Comput Methods Eng Sci Mech 2022;23:29–44.
[42] Freddi F, Mingazzi L. Mesh refinement procedures for the phase field approach to brittle fracture. Comput Methods Appl Mech Engrg 2022;388:114214.
[43] Freddi F, Mingazzi L. Adaptive mesh refinement for the phase field method: A FEniCS implementation. Appl Eng Sci 2023;14:100127.
[44] Amor Hanen, Marigo Jean Jacques, Maurini Corrado. Regularized formulation of the variational brittle fracture with unilateral contact: Numerical experiments. J Mech Phys Solids 2009;57(8):1209–29.
[45] Farrell Patrick, Maurini Corrado. Linear and nonlinear solvers for variational phase-field models of brittle fracture. Internat J Numer Methods Engrg 2017;109:648–67.
[46] Geuzaine Christophe, Remacle Jean-François. Gmsh: A 3-D finite element mesh generator with built-in pre- and post-processing facilities. Internat J Numer Methods Engrg 2009;79(11):1309–31.
[47] Prasad NNV, Aliabadi MH, Rooke DP. Incremental crack growth in thermoelastic problems. Int J Fract 1994;R45–50, 66.
[48] Duflot M. The extended finite element method in thermoelastic fracture mechanics. Internat J Numer Methods Engrg 2008;74:827–47.
[49] Sarkar Subrato, Singh IV, Mishra BK. A Thermo-mechanical gradient enhanced damage method for fracture. Comput Mech 2020;66(6):1399–426.
[50] Mandal Tushar Kanti, Nguyen Vinh Phu, Wu Jian-Ying, Nguyen-Thanh Chi, de Vaucorbeil Alban. Fracture of thermo-elastic solids: Phase-field modeling and new results with an efficient monolithic solver. Comput Methods Appl Mech Engrg 2021;376:113648.
[51] Wang HS. A meshfree variational multiscale methods for thermo-mechanical material failure. Theor Appl Fract Mech 2015;75:1–7.
[52] Wang Tao, Ye Xuan, Liu Zhanli, Liu Xiaoming, Chu Dongyang, Zhuang Zhuo. A phase-field model of thermo-elastic coupled brittle fracture with explicit time integration. Comput Mech 2020;65(5):1305–21.
[53] Shao Yingfeng, Zhang Yue, Xu Xianghong, Zhou Zhiliang, Li Wei, Liu Boyang. Effect of crack pattern on the residual strength of ceramics after quenching. In: Jin Z-H, editor. J Am Ceram Soc 2011;94(9):2804–7.
[54] Jiang CP, Wu XF, Li J, Song F, Shao YF, Xu XH, et al. A study of the mechanism of formation and numerical simulations of crack patterns in ceramics subjected to thermal shock. Acta Mater 2012;60:4540–50.
[55] Chu Dongyang, Li Xiang, Liu Zhanli. Study the dynamic crack path in brittle material under thermal shock loading by phase field modeling. Int J Fract 2017;208(1–2):115–30.
[56] Li Yicong, Yu Tiantang, Xing Chen, Natarajan Sundarajan. Modeling quasi-static and dynamic thermo-elastic coupled brittle fracture using an adaptive isogeometric hybrid phase-field method. Finite Element Anal Des 2023;224:103993.
[57] Stopyra Wojciech, Gruber Konrad, Smolina Irina, Kurzynowski Tomasz, Kuźnicka Bogumiła. Laser powder bed fusion of AA7075 alloy: Influence of process parameters on porosity and hot cracking. Addit Manuf 2020;35:101270.